Indian Journal of Pure & Applied Physics
Vol. 53, August 2015, pp. 530-536

Preparation and thermoelectric properties of the rare earths doped $Ca_{0.95}RE_{0.05}MnO_3$ (RE=Pr, Eu and Tb) oxide materials

Z N Jiang[1], F P Zhang[2,3,*], X Zhang[3], Q M Lu[3] & J X Zhang[3]

[1]Department of Physics and Electronic Engineering, Guangxi Normal University for Nationalities, 532200, Chongzuo, Guangxi, People's Republic of China

[2]Institute of Physics, Henan University of Urban Construction, 467036, Henan, People's Republic of China

[3]National Key Laboratory of Advanced Functional Materials, Chinese Ministry of Education, College of Materials Science and Engineering, Beijing University of Technology, 100124, Beijing, People's Republic of China

*E-mail: zhfp@emails.bjut.edu.cn; zhfp163@163.com

Received 17 March 2014; revised 20 May 2014; accepted 19 March 2015

The rare earths doped $Ca_{0.95}RE_{0.05}MnO_3$ (RE=Pr, Eu, Tb) oxide bulk materials are fabricated and the effects of rare earths doping within low content on the thermoelectric transport properties of the $CaMnO_3$ oxide have been investigated. The results show that all doped oxide bulk materials are single phase with consolidated microstructure. The electrical resistivity is remarkably reduced on account of electron carrier density and mobility enhancement. The Seebeck coefficient is simultaneously reduced and the total thermal conductivity is decreased due to phonon thermal conduction confinement. The thermoelectric figure of merit *ZT* is improved with peak values of 0.12, 0.12 and 0.09 at 973 K for the Pr, Eu and Tb doped $CaMnO_3$ oxide materials, respectively, which are very much higher than that of the undoped oxide material.

Keywords: $CaMnO_3$ oxide, Rare earth doping, Thermoelectric properties

1 Introduction

Thermoelectric (TE) materials can convert heat energy into electrical energy directly[1-4]. They have many potential application areas for converting various kinds of heat energy into electricity, including solar heat, geothermal heat and the exhaust heat of automobiles. They have been receiving continuous attention due to the energy crisis worldwide during the past years for their advantages of solid-state operation, vast scalability, zero emissions, no maintenance and long lifetime. The performance of a TE material is evaluated by the following function as:

$$ZT=\alpha^2 T/\rho\kappa \quad \ldots(1)$$

where α is Seebeck coefficient, ρ the electrical resistivity, κ the total thermal conductivity, T the absolute temperature and ZT is the dimensionless figure of merit, respectively[2-4]. Good TE materials should have simultaneously high Seebeck coefficient α, low resistivity ρ and thermal conductivity κ in order to achieve a considerably high dimensionless figure of merit ZT. Great development has been achieved for some alloys-based TE materials, such as the tellurides[3-6], antimonides[3,4], skutterudites[7], silicides[8], clathrates[9]and half-Heusler alloys[7]. The tellurides and antimonides have been regarded as the most prospective TE materials; they have ZT value of unit near room temperature. Unfortunately, the high cost, instability and toxicity of these materials are inevitable problems for high temperature application[10]. Oxide based TE materials are being paid more and more attention in recent years for their cheap raw materials, easy fabrication and anti-atmospheric-induced decomposition characteristics. The transition metal oxide materials have received increasingly much attention for their potential TE properties and other physical phenomena[10-14]. Among these type of oxide materials, the transition metal oxide $CaMnO_3$ exhibits sensitively tunable resistivity, relatively low thermal conductivity and high Seebeck coefficient[12,13] ($|\alpha_{300K}| \approx 350\ \mu\cdot V\cdot K^{-1}$). It has been the hotspot within TE fields during the past decade due to its potential performance and application in energy conversion areas such as waste heat power generation and heat collection in industry production process[14-16]. An averaged ZT value of 1.15 at 1000 K is theoretically obtained for the single crystal material, predicting its greatly potential applications. However, the TE performance of polycrystalline

$CaMnO_3$ material is relatively low ($ZT<0.5$); much work should be done to improve the TE property of the polycrystalline $CaMnO_3$ oxide material.

The dimensionless figure of merit *ZT* is a combined function of electrical transport parameters and thermal transport parameters such as carrier concentration, carrier mobility, the type of carrier, as well as the vibrational mode, phonon mean free path, phonon density of states and scattering mechanism. These parameters are not independent; they are closely correlated to each other. Doping is proved to be a successful way tuning these parameters[17-20]. It has been verified that the electrical and thermal transport properties can be successfully optimized[14,16,19,20] by doping for Ca and the figure of merit *ZT* can thus be enhanced.

The rare earths doping for Ca should theoretically introduce electron carriers in the $CaMnO_3$ system. Secondly, the rare earths have high atomic mass and comparable ionic radius with Ca, the rare earths doping for Ca should lower the phonon mean free path and the velocity, this is favourable for reducing the phonon thermal conductivity. It is hopefully estimated that the rare earths doping for Ca should optimize the electrical and thermal properties, thereafter an elevated figure of merit *ZT* can be obtained. It has been verified within former works that the electrical and thermal transport properties were successfully tuned, the TE performance was indeed improved by rare earths doping. A *ZT* of 0.16 at 1100 K was reported for the Pr doped $CaMnO_3$ oxide materials at a lower content[21], indicating that the rare earths doping for Ca within low content should optimize the TE properties of the titled system. At the same time, the nitrates of Pr, Eu and Te are relatively cheap and they can be easily prepared. In order to systematically investigate the effects of serial rare earths doping within lower content on TE properties of the $CaMnO_3$ oxide material systems, the rare earths Pr, Eu and Tb doped polycrystalline $Ca_{0.95}RE_{0.05}MnO_3$ (RE=Pr, Eu, Tb) oxide material samples are prepared in the present work. The effects of rare earths doping for Ca within lower content on TE transport properties of $CaMnO_3$ oxide material system have been systematically studied.

2 Experimental Details

The rare earths doped $Ca_{0.95}RE_{0.05}MnO_3$ (RE=Pr, Eu, Tb) oxide bulk materials were prepared by citrate acid sol-gel reaction and modified ceramics preparation method. Stoichiometric ratios of highly pure nitrates of Ca, Pr, Eu, Tb and Mn were dissolved in distilled water and the citric acid was added in the aqueous solution. The solution was continuously mixed and heated at 360K for 15h in order to form the precursor gel. The gel was firstly dried at 428 K for 48h in air to evaporate the excessive water, and then the resulting gel was dried at 473 K for 12 h to allow for full inflation. Then, the dried gel was finely ground and calcined at 1173 K for 8h to remove excess organic compounds and get the $Ca_{0.95}RE_{0.05}MnO_3$(RE=Pr, Eu, Tb) ceramic powder. Then the powder was finely ground and pressed into platelets under a uniaxial pressure of 500MPa. Finally, the pressed platelets were heated slowly to the temperature of 1473 K in air at the heating rate of 10K/min and the specimens were maintained at 1473 K for 12 h. Then the specimens were subjected to furnace cooling from 1473 K to room temperature. The specimens were subjected to flowing air in atmospheric pressure during the bulk specimen preparation process.

The phase compositions of bulk specimens were analyzed by X-ray diffraction (XRD) at room temperature on a Rigaku diffractometor with CuK_α radiation in a 2 theta range 20°~85°, with steps of 0.02°(2θ) and a time per step of 1s. The microscopic image of the bulk specimens was obtained with the scanning electron microscope (SEM) using secondary electron mode by Nova NanoSEM operated at 18KV. The electrical resistivity and Seebeck coefficient were measured in He atmosphere from room temperature up to 1000 K using a conventional *dc* standard four-probe method on ULVAC ZEM-2 system. The thermoelectric potential difference ΔE was measured for an applied temperature difference ΔT of 20 K to 40 K. The Seebeck coefficient α was obtained from the slope of ΔE versus ΔT. The specific heat capacity C and thermal diffusivity λ were measured in He atmosphere by the laser flash technique on ULVAC-RIKO TC-7000 system. The density d was measured by Archimedes method. Then the total thermal conductivity κ was calculated by $\kappa=dC\lambda$. The Hall coefficients R_H of the bulk samples were measured at room temperature using an integrated property measurement system (PPMS-9) at a magnetic field of 0.1T controlled by liquid-nitrogen cooling and a microcavity sample heater. The carrier density n was obtained using the formula $N_e = 1/eR_H$ (where e is the charge of the electron).

3 Results and Discussion

3.1 Bulk Material Phase Composition

The room temperature XRD patterns of the rare earths doped $Ca_{0.95}RE_{0.05}MnO_3$ (RE=Pr, Eu, Tb) oxide bulk materials are shown in Fig. 1. The reflections observed for all oxide materials can be well indexed in perovskite type $CaMnO_3$ by comparing with $CaMnO_3$ (JCPDS card No. 50-1746), indicating that the orthorhombic type compound solid solutions with *pnma* symmetry are formed for all oxide materials.

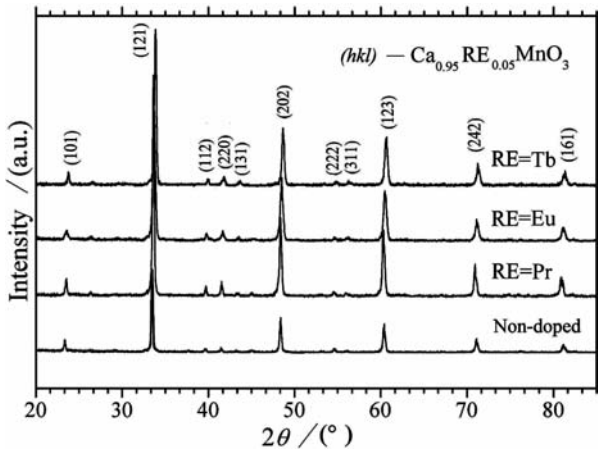

Fig. 1 — XRD patterns of all the oxide bulk materials

3.2 Bulk Material Microstructure

Figure 2 shows the fractured cross-section SEM images for all bulk materials. Since the preparation procedure is the same and parallel, the evaluation of all the bulk materials is reasonable. It is observed that all the bulk specimens have consolidated microstructures, with a few porosities at the boundaries of the $Ca_{0.95}RE_{0.05}MnO_3$ grains. The measured densities are 4.22, 4.33 and 4.35 $g.cm^3$ for the Pr, Eu and Tb doped bulk materials, respectively, which are roughly higher than that of the undoped samples 4.18 $g.cm^3$. They show similar compact bulk microstructures, and the relationship between microstructures and dopants is weak.

3.3 Electrical Properties

The electrical resistivity ρ, Seebeck coefficient α and power factor P as a function of temperature for the rare earths doped $Ca_{0.95}RE_{0.05}MnO_3$ (RE=Pr, Eu, Tb) oxide materials are shown in Fig. 3. It could be observed that the electrical resistivity is sensitively modulated by rare earths doping. The resistivity for

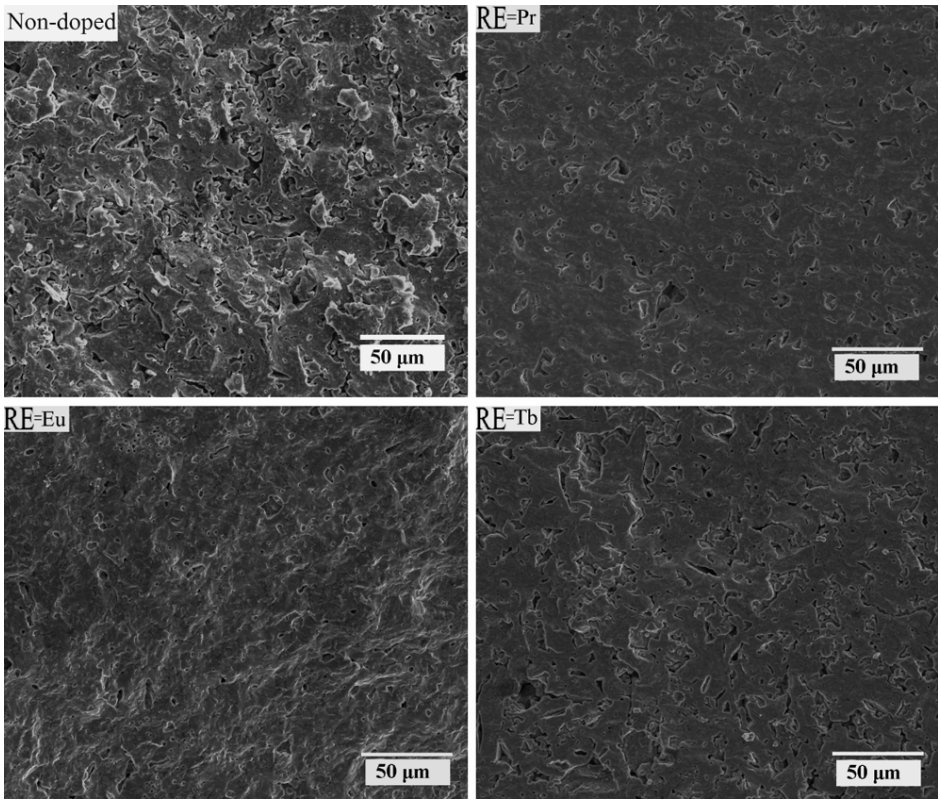

Fig. 2 — Fractured cross-section SEM images of the un-doped and doped $Ca_{0.95}RE_{0.05}MnO_3$ (RE=Pr, Eu, Tb) oxide bulk materials

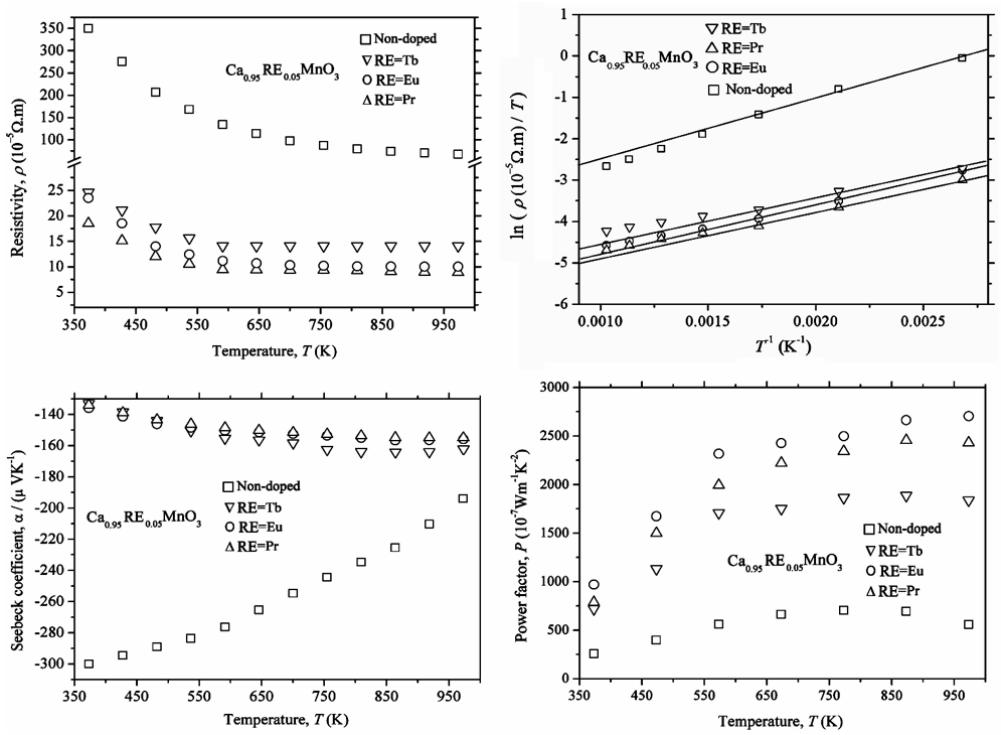

Fig. 3 — Electrical resistivity ρ, ln (ρ/T) versus 1/T, Seebeck coefficient α and power factor P as a function of temperature of all the oxide bulk materials

the undoped sample is relatively high and it decreases with increasing temperature, indicating its semiconductor nature. The resistivity of the rare earths doped samples is notably decreased and it is also decreased with increasing temperature. For instance, the resistivity at 373 K is $350.1\times10^{-5}\Omega$.m for the undoped $CaMnO_3$ sample, it is decreased to $18.3\times10^{-5}\Omega$.m, $23.8\times10^{-5}\Omega$.m and $24.6\times10^{-5}\Omega$.m for the Pr, Eu as well as the Te doped samples, respectively. The $CaMnO_3$ system has theoretically an indirect band gap[21,22] of 0.7eV, the resistivity ρ for a semiconductor system can be expressed according to the following equation:

$$\rho \propto \frac{1}{ne\mu} \qquad \ldots(2)$$

where the n is carrier density, e the elementary charge and μ is mobility[23]. The main carriers for orthorhombic $CaMnO_3$ oxide are electrons, doping with rare earths for Ca site should contribute electron carriers into the system, the carrier density n would be enhanced, thus the resistivity is decreased. This phenomenon can also be explained by associating with the electronic structure according to:

Table1 — Resistivity ρ at 373 K and room temperature carrier density n and mobility μ of all the oxide bulk materials

RE	$p/10^{-5}\Omega$m	$n/10^{19}$ cm^{-3}	μ/cm^2/Vs
Ca	350.1	1.02	2.8
Pr	18.3	1.28	7.0
Eu	23.8	1.25	6.1
Tb	24.6	1.13	5.8

$$n \propto n_0 \exp\left[\frac{(E_F - E_{F0})}{k_B T}\right] \qquad \ldots(3)$$

where n_0 and E_{F0} are the carrier density and Fermi level of the undoped sample, E_F the Fermi level of the doped sample, k_B Boltzman constant and the T is the temperature. The Fermi level can be shifted towards the conduction band by electron donor doping, thus the carrier density n is larger than that of the undoped sample. In order to validate the theoretical estimation, Table 1 presents the resistivity at 373 K, the measured room temperature carrier concentration n and mobility μ for all samples. It is obviously shown that the carrier concentration n is increased; the mobility μ is also enhanced. For instance, the n is increased from 1.02×10^{19} cm^{-3} of the

undoped sample to 1.28×10^{19} cm^{-3} of the Pr doped sample. At the same time, the μ is increased from 2.8 cm^2/Vs of the undoped sample to 7.0 cm^2/Vs of the Pr doped sample. The resistivity of the $CaMnO_3$ is decreased on account of increased electron carrier concentration and the enhanced mobility[24].

There are several models describing the transport behaviour of the oxide materials. Energies for localized carriers to motivate as moving carriers are important and these deserve investigations. In the present work, the temperature dependence of electrical resistivity ρ for the titled oxide material system can be simulated by the small polaron model according to the transport theory proposed by Mott expressed as:

$$\rho(T) \propto C\,T \exp(E_a/k_BT) \qquad \ldots(4)$$

where E_a is the activation energy of the polarons, k_B the Boltzman constant, T is the absolute temperature, and the C could be regarded as a constant[12,13]. Figure 3 shows that the plots of ln (ρ/T) versus $1/T$ for all samples lie on the straight lines within the whole temperature region; this verifies the applicability of the transport model. By calculating the slopes of the linear fit of ln (ρ/T) versus $1/T$, the activation energy E_a of the polarons can be obtained. The value E_a is decreased from 0.09eV of the undoped $CaMnO_3$ to approximately 0.07eV of the doped samples. This corresponds to the modified electronic structure of the doped oxide materials. New energy bands should be generated within the band gap by the donor doping[27]. The energy for carriers to hop is lowered and the resistivity is decreased.

The Seebeck coefficient α values for all the samples are negative, confirming that the electron carriers are dominant for the titled oxide material system. The absolute value of Seebeck coefficient of the undoped sample is relatively high and it decreases with increasing temperature, in agreement with its electrical resistivity behaviour which is related to the low carrier concentration and semiconductor nature of the undoped $CaMnO_3$ oxide system. The absolute values of Seebeck coefficients for the rare earths doped samples are notably decreased comparing with the undoped sample within the whole measuring temperature region. This phenomenon can be explained by the changed carrier concentration and mobility. The absolute value of Seebeck coefficient for the $CaMnO_3$ oxide can be regarded as a function of the carrier concentration n and the carrier mobility μ:

$$a \propto \frac{\pi^2}{3}\left[\frac{{k_B}^2 T}{q}\right]\left[\frac{1}{n}\frac{dn(E)}{d(E)} + \frac{1}{\mu}\frac{d\ln\mu(E)}{d(E)}\right]_{E=E_F} \qquad \ldots(5)$$

where n, μ, $n(E)$, $\mu(E)$, k_B and E_F are carrier concentration, mobility, energy correlated carrier concentration, energy correlated carrier mobility, Boltzmann constant and Fermi energy, respectively[28]. The formula consists of two terms, the value of the first term n is carrier concentration and the second term μ is the mobility. The rare earths doping increases the carrier concentration n and the mobility μ at the same time, therefore, the Seebeck coefficient is decreased. It can also be observed that the absolute values of Seebeck coefficients for the rare earths doped samples are increased with increasing temperature. The absolute value of Seebeck coefficient as a function of temperature for the semiconductor materials system could be expressed as follows:

$$a \propto \frac{m^* k_B^2}{h^2}\left(\frac{1}{n}\right)^{2/3} T \qquad \ldots(6)$$

where m^* and h are the effective mass of the carriers and the Planck constant, respectively[7,11]. The doped sample shows good agreement with the model that the Seebeck coefficient is enhanced with increasing temperature. The absolute value of Seebeck coefficient for the rare earths doped oxide materials is decreased. This is a well explanation that the Seebeck coefficient is a reverse function of carrier concentration n.

Figure 3 shows that the undoped sample exhibits very low power factor on accounts of its high resistivity. The power factors of doped oxide samples are higher than that of the undoped oxide system, they reach 2500×10^{-7}, 2755×10^{-7} and 1750×10^{-7} $Wm^{-1}K^{-2}$ at 973 K for the Pr, Eu and Tb doped systems, respectively. It can also be seen that the power factor P for doped samples is increased remarkably with increasing temperature and the P value could be even higher at higher temperature, indicating the rapidly enhanced electrical performance with increasing temperature.

3.4 Thermal Transport Properties

Figure 4 shows the measured thermal conductivity k. It is obvious that the κ values for the rare earths doped $Ca_{0.95}RE_{0.05}MnO_3$ (RE=Pr, Eu, Tb) oxide materials are considerably lower than that of the

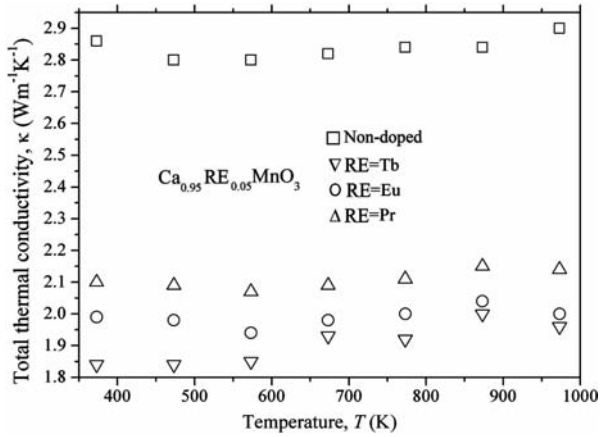

Fig. 4 — Thermal conductivity κ as a function of temperature of all the oxide bulk materials

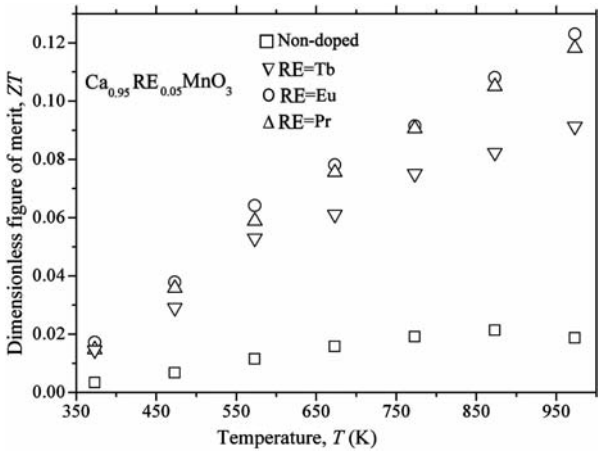

Fig. 5 — Figure of merit *ZT* as a function of temperature of all the oxide bulk materials

undoped material. The total thermal conductivity is regarded as composing of the carrier thermal conductivity term k_e and the phonon thermal conductivity term k_L. The total thermal conductivity is mainly composed of the phonon thermal conductivity for the titled oxide material system[14,16,21]. The phonon thermal conductivity k_L for crystalline phase material is a function of heat capacity c_v, phonon mean free path λ_L and phonon velocity v expressed[26,27] as:

$$k_L \propto c_v v \lambda_L \qquad \ldots(7)$$

The phonon mean free path λ_L can be lowered by heavy elements doping, the density of high frequency optical phonon modes should also be decreased which leads to the decrease of phonons that carries heat effectively[27,29]. The suppression of thermal conductivity can be explained by that the phonon mean free path λ_L is made much more finite and the velocity v is made lower through heavy elements doping, the vibration modes that carry heat efficiently are decreased, and therefore the thermal conductivity is reduced.

3.5 Figure of Merit, ZT

Figure 4 shows the dimensionless figure of merit *ZT* value as a function of temperature for all the oxide material systems. The *ZT* values increase with increasing temperature, indicating their potential application within high temperature region. The *ZT* values for doped systems are very much higher than that of the undoped system, reaching peak values of 0.12, 0.12 and 0.09 at 973 K for the Pr, Eu and Tb doped $CaMnO_3$ oxide materials, respectively. Secondly, the *ZT* values for doped materials increase much more rapidly with increasing temperature by comparing with the undoped material. The TE performance should be even higher at higher temperature above 973 K for rare earths doped material systems (Fig. 5).

4 Conclusions

The TE transport properties of the rare earths doped $Ca_{0.95}RE_{0.05}MnO_3$ (RE=Pr, Eu, Tb) oxide materials have been studied. All oxide materials are found to be single phase in orthorhombic symmetry. The bulk materials show consolidated microstructures, with existence of small porosities. The electrical resistivity is decreased remarkably by rare earths doping as a result of carrier density and mobility enhancement and the Seebeck coefficient is deteriorated at the same time. The thermal conductivity is reduced considerably, the TE performance is improved with peak *ZT* values of 0.12, 0.12 and 0.09 at 973 K for the Pr, Eu and Tb doped $CaMnO_3$ oxide materials, respectively, which are very much higher than that of the undoped material. The present investigation verified that the rare earths doping within low content is indeed an effective way for improving TE performance of the $CaMnO_3$ oxide material system.

Acknowledgement

This work is financially supported by the National Natural Science Foundation of China under Grant No. 50801002, the Scientific Research Project of Guangxi Normal University of Nationalities under Grant No. 2013ZDa001, the Teaching Reform Research

Project of Guangxi Normal University of Nationalities under Grant No. SFZX201102 and the Scientific Research Project of Guangxi Universities under Grant No. 2013YB268.

References

1 Zhao L D, Lo S H, Zhang Y S, Sun H, Tan G J, Uher C, Wolverton C, Dravid V P & Kanatzidis M G, *Nature*, 508 (2014) 373.
2 Li J F, Liu W S, Zhao L D & Zhou M, *N P G Asia Mater,* 2 (2010) 152.
3 Walia S, Weber R, Sriram S, Bhaskaran M, Latham K, Zhuiykov S & Kalantar-Zadeh K, *Energy & Environ Sci,* 4 (2011) 3558.
4 Venkatasubramanian R, Siivola E, Colpitts T & Quinn BO, *Nature,* 413 (2001) 597.
5 Dresselhaus M S, Chen G, Tang M Y, Yang R G, Lee H, Wang D Z, Ren Z F, Fleurial J P & Gogna P, *Adv Mater*, 19 (2007) 1043.
6 Walia S, Weber R, Latham K, Petersen P, Abrahamson J T, Strano M S & Kalantar-Zadeh K, *Adv Funct Mater,* 21 (2011) 2072.
7 Snyder G Jeffrey & Toberer Eric S, *Nature Mater*, 7 (2008) 105.
8 Hauser D, Savelli G, Plissonnier M, Montès L & Simon J, *Thin Solid Films*, 520 (2012) 4259.
9 Saiga Y, Suekuni K, Du B & Takabatake T, *Solid State Commun*, 152 (2012) 1902.
10 Walia S, Balendhran S, Nilli H, Zhuiykov S, Rosengarten G, Wang Q H, Sriram S, Bhaskaran M, Strano M S & Kalantar-Zadeh K, *Prog Mater Sci,* 58 (2013) 1443.
11 Walia S, Balendhran S, Yi P, Yao D, Zhuiykov S, Pannirselvam M, Weber R, Strano M S, Bhaskaran M, Sriram S & Kalantar-Zadeh K, *J Phys Chem C*, 117 (2013) 9137.
12 Miclau M, Hébert S & Retoux R, *J Solid State Chem*, 178 (2005) 1104.
13 Matsukawa M, Tamura A & Yamato Y, *J Magn Magn Mater,* 310 (2007) 283.
14 Fergus J F, *J Euro Ceram Soc,* 32 (2012) 525.
15 Zhang F P, Lu Q M, Zhang X & Zhang J X, *J Phys Chem Solids,* 74 (2013) 1859.
16 Huang X Y, Miyazaki Y & Kajitani T, *Solid State Commun,* 145 (2007) 132.
17 Zhou Q & Kennedy B J, *J Phys Chem Solids,* 67 (2006) 1595.
18 Wollan E O & Koehler W C, *Phys Rev,* 100 (1955) 545.
19 Zeiske Th, Hagdorn K, Hohlwin D, Ihringer J, Prandl W & Ritter H, *Physica* B, 276 (2000) 624.
20 Maignan A, Martin C, Damay F & Raveau B, *Chem Mater,* 10 (1998) 950.
21 Cong B T, Toshihide T, Pham X T, Phung Q T & Yasuhisa Y, *Physica* B, 352 (2004) 18.
22 Zhang F P, Lu Q M, Zhang X & Zhang J X, *J Alloys Compd,* 509 (2011) 542.
23 Zhao L D, Zhang B P, Li J F, Zhang H L & Liu W S, *Solid State Sci,* 10 (2008) 651.
24 Zhang X, Liu H L, Lu Q M, Zhang J X & Zhang F P, *Appl Phys Lett,* 103 (2013) 063901.
25 Jiang J, Chen L, Bai S & Yao Q, *J Alloys Compd,* 390 (2005) 208.
26 Li J C, Wang C L, Wang M X, Pen H, Zhang R Z, Zhao M L, Liu J, Zhang J L & Mei L M, *J Appl Phys,* 105 (2009) 043503.
27 Li J C, Wang C L, Peng H, Wang M X, Zhang R Z, Wang H C, Liu J, Zhao M L & L Mei M, *J Appl Phys,* 108 (2010) 063702.
28 Maignan A, Martin C, Damay F & Raveau B, *Phys Rev* B, 58 (1998) 2758.
29 Shi X, Hong H, Li C P, Uher C, Yang J, Salvador J R, Wang H, Chen L & Zhang W, *Appl Phys Lett,* 92 (2008) 182101.